PHYSICAL REVIEW D **79,** 073010 (2009)

Light sterile neutrinos, spin flavor precession, and the solar neutrino experiments

C. R. Das* and João Pulido†

Centro de Física Teórica das Partículas (CFTP), Departamento de Física, Instituto Superior Técnico Av. Rovisco Pais, P-1049-001 Lisboa, Portugal

Marco Picariello‡

I.N.F.N. - Lecce, and Dipartimento di Fisica, Università di Lecce, Via Arnesano, ex Collegio Fiorini, I-73100 Lecce, Italia

(Received 12 February 2009; published 16 April 2009)

We generalize to three active flavors a previous two-flavor model for the resonant spin flavor conversion of solar neutrinos to sterile ones, a mechanism which is added to the well-known large mixing angle (LMA) one. The transition magnetic moments from the muon and tau neutrinos to the sterile play the dominant role in fixing the amount of active flavor suppression. We also show, through numerical integration of the evolution equations, that the data from all solar neutrino experiments except Borexino exhibit a clear preference for a sizable magnetic field either in the convection zone or in the core and radiation zone. This is possibly related to the fact that the data from the first set are average ones taken during a period of mostly intense solar activity, whereas in contrast Borexino data were taken during a period of quiet Sun. We argue that the solar neutrino experiments are capable of tracing the possible modulation of the solar magnetic field. Those monitoring the high-energy neutrinos, namely, the ^{8}B flux, appear to be sensitive to a field modulation either in the convection zone or in the core and radiation zone. Those monitoring the low-energy fluxes will be sensitive to the second type of solar field profiles only. In this way Borexino alone may play an essential role, since it examines both energy sectors, although experimental redundancy from other experiments will be most important.

DOI: 10.1103/PhysRevD.79.073010 PACS numbers: 14.60.Pq

I. INTRODUCTION AND MOTIVATION

Although the effort in solar neutrino investigation has decreased in recent years, several intriguing questions in this area remain open. Their clarification may lead to a better knowledge of the neutrino intrinsic properties, the structure of the inner solar magnetic field, or possibly both. In fact it is still unclear, for example, whether the active solar neutrino flux varies in time [1–4] or why the Super-Kamiokande energy spectrum appears to be flat [5,6]. The generally acknowledged large mixing angle (LMA) solution [7] to the neutrino deficit observed by all solar neutrino experiments does not explain these facts, while it further predicts an event rate for the Chlorine experiment [8], which is 2σ above the observed one [9]. These could be indications of physics beyond LMA.

Based on this motivation and in line with the originally proposed resonant spin flavor precession of solar neutrinos [10,11], we were led to develop a model whereby neutrinos are endowed with a transition magnetic moment converting active into sterile ones by virtue of their interaction with the magnetic field of the Sun [12]. In particular we considered a scenario in which the apparently time-varying event rate of the Gallium experiments [13,14] was viewed in connection with the solar magnetic activity [15]. Owing to the uncertainties involved, such data are however also consistent with a constant Ga rate, which is the alternative conventional view we will consider in the present paper. It is also possible to generate time variations of the active neutrino flux using the parametric resonance for matter density perturbations in the presence of a radiation zone magnetic field without resorting to magnetic moments or sterile neutrinos [16].

The model expound in Refs. [12,15] considered two resonances, the LMA one between two oscillating active neutrinos and the spin flavor precession one determined by a transition moment between one of the active flavors and the sterile one. The location of the active-sterile resonance, near the bottom of the solar convection zone, was fixed by the corresponding active-sterile mass squared difference which for this purpose was chosen to be $O(10^{-8} - 10^{-9})$ eV^2. The survival and transition probabilities were calculated using the Landau-Zener approximation.

In this paper we extend our previous model with two active flavors and one sterile to the more realistic case of three active flavors and a sterile. Whereas the Landau-Zener approximation works well in the LMA resonance, this is not so for spin flavor precession, thus we will resort to the numerical integration of the evolution equations. However the best-fit parameter values are obtained from the Landau-Zener approximation, as they are found to coincide in both methods. We take several values of θ_{13} in the allowed range for both strong and weak solar fields. The model event rates for all solar neutrino experiments are evaluated and confronted with the data. Special emphasis is given to the Super-Kamiokande energy spectrum

*crdas@cftp.ist.utl.pt
†pulido@cftp.ist.utl.pt
‡Marco.Picariello@le.infn.it

[6] and the recent ^{8}B energy spectrum from the Borexino experiment [17]. We consider two classes of solar field profiles, whose field strengths peak in the solar core (Wood-Saxon potential type) and in the lower convection zone. Together these span a large number of possibilities.

The paper is organized as follows: in Sec. II the derivation of the (4×4) Hamiltonian in the mass eigenstate basis is presented. In Sec. III A the already known fact that the survival probability is a decreasing function of θ_{13} is shown to follow from a simple argument. In Sec. III B the evaluation of the event rates and spectra is presented. The results are discussed in Sec. III C. Finally in Sec. IV our conclusions are drawn. Our numerical calculations are based on the updated central values [18] for Δm^2_{21}, θ_{12}, θ_{23}, Δm^2_{32} and we use a neutrino transition moment between flavor states not larger than $\mu_\nu = 1.4 \times 10^{-12} \mu_B$. As for θ_{13} we chose to investigate three cases: $\theta_{13} = 0$, 0.1, and the central value, 0.13. The fits to all data, including rates and spectra (except for Borexino), improve once the magnetic field is introduced. As regards Borexino, the fit worsens in this case. This may be connected to the fact that all former experiments report time averaged data taken during times of more or less intense solar magnetic activity, whereas Borexino data were taken during a period of minimum activity. In contrast, solar data alone show no clear preference for a vanishing or sizable θ_{13}.

II. THE HAMILTONIAN

The (4×4) Hamiltonian involving one sterile neutrino and three active ones will be expressed in the mass eigenstate basis. This is related to the flavor basis by

$$\begin{pmatrix} \nu_S \\ \nu_e \\ \nu_\mu \\ \nu_\tau \end{pmatrix} = U^{\rm PMNS}(4 \times 4) \begin{pmatrix} \nu_0 \\ \nu_1 \\ \nu_2 \\ \nu_3 \end{pmatrix} \tag{1}$$

where $U^{\rm PMNS}$ (4×4) is the straightforward (4×4) extension of the usual leptonic mixing matrix [19]. As before [12,15] no vacuum mixing between the sterile and any of the active flavors is assumed, so that the free propagating term of the Hamiltonian is in the mass basis

$$(H_0)_M = \begin{pmatrix} E_0 & & & \\ & E_1 & & \\ & & E_2 & \\ & & & E_3 \end{pmatrix} \tag{2}$$

and the matter (interaction) term is in the flavor basis

$$(H_I)_W = \begin{pmatrix} 0 & \mu_{es}B & \mu_{\mu s}B & \mu_{\tau s}B \\ \mu_{es}B & V_c + V_n & 0 & 0 \\ \mu_{\mu s}B & 0 & V_n & 0 \\ \mu_{\tau s}B & 0 & 0 & V_n \end{pmatrix}. \tag{3}$$

Here $\mu_{(e,\mu,\tau)s}$ are the transition magnetic moments between the active flavors and the sterile one and B is the magnetic field profile. The quantities V_c, V_n are the refraction indexes for charged and neutral currents, namely $V_c = G_F\sqrt{2}N_e$, $V_n = -(G_F/\sqrt{2})N_n$ with N_e (electron density) and N_n (neutron density). Given Eq. (1), the mass and flavor Hamiltonian representations are related by

$$H_M = U^{\dagger \rm PMNS} H_W U^{\rm PMNS} \tag{4}$$

so that the full Hamiltonian in the mass basis is

$$H_M = \begin{pmatrix} E_0 & & & \\ & E_1 & & \\ & & E_2 & \\ & & & E_3 \end{pmatrix} + U^{\dagger \rm PMNS} \begin{pmatrix} 0 & \mu_{es}B & \mu_{\mu s}B & \mu_{\tau s}B \\ \mu_{es}B & V_c + V_n & 0 & 0 \\ \mu_{\mu s}B & 0 & V_n & 0 \\ \mu_{\tau s}B & 0 & 0 & V_n \end{pmatrix} U^{\rm PMNS}. \tag{5}$$

Subtracting E_1 and denoting by $\tilde{\mu}_{1,2,3}$ the transition magnetic moment between mass eigenstates 0 and 1, 2, 3, respectively, we have

$$H_M = \begin{pmatrix} \frac{\Delta m^2_{01}}{2E} & \tilde{\mu}_1 B & \tilde{\mu}_2 B & \tilde{\mu}_3 B \\ \tilde{\mu}_1 B & 0 & 0 & 0 \\ \tilde{\mu}_2 B & 0 & \frac{\Delta m^2_{21}}{2E} & 0 \\ \tilde{\mu}_3 B & 0 & 0 & \frac{\Delta m^2_{31}}{2E} \end{pmatrix} + U^{\dagger \rm PMNS} \begin{pmatrix} 0 & 0 & 0 & 0 \\ 0 & V_c + V_n & 0 & 0 \\ 0 & 0 & V_n & 0 \\ 0 & 0 & 0 & V_n \end{pmatrix} U^{\rm PMNS}. \tag{6}$$

Straightforward matrix algebra leads now to

$$H_M = \begin{pmatrix} \frac{\Delta m^2_{01}}{2E} & \tilde{\mu}_1 B & \tilde{\mu}_2 B & \tilde{\mu}_3 B \\ \tilde{\mu}_1 B & V_n + V_c u^2_{e_1} & V_c u_{e_1} u_{e_2} & V_c u_{e_1} u_{e_3} \\ \tilde{\mu}_2 B & V_c u_{e_1} u_{e_2} & \frac{\Delta m^2_{21}}{2E} + V_n + V_c u^2_{e_2} & V_c u_{e_2} u_{e_3} \\ \tilde{\mu}_3 B & V_c u_{e_1} u_{e_3} & V_c u_{e_2} u_{e_3} & \frac{\Delta m^2_{31}}{2E} + V_n + V_c u^2_{e_3} \end{pmatrix} \tag{7}$$

where u_{e_i} denotes the first row entries of the (3×3) $U^{\rm PMNS}$ matrix. In the following we assume vanishing phases. Equation (7) is the mass basis Hamiltonian that we use throughout.

III. PROBABILITY AND RATES

A. 3 Flavor probability and θ_{13}

A simple argument shows that the electron neutrino survival probability for three active flavors [20,21]

$$P_{3\times3}(\nu_e \to \nu_e) = \cos^4\theta_{13} P_{2\times2}(\nu_e \to \nu_e(N_e \to N_e\cos^2\theta_{13})) + \sin^4\theta_{13} \quad (8)$$

where extra terms $O(10^{-3})$ or smaller have been neglected [21] is a decreasing function of θ_{13}. In Eq. (8) the (2×2) probability with the replacement $N_e \to N_e\cos^2\theta_{13}$ is given by [21]

$$P_{2\times2} = \frac{1}{2} + \frac{1}{2}\cos2\theta_{12}\frac{-\phi(x)}{\sqrt{(\frac{\Delta m^2_{21}}{4E}\sin2\theta_{12})^2 + \phi^2}} \quad (9)$$

where x is the fractional solar radius and

$$\phi = \frac{G_F}{\sqrt{2}}N_e\cos^2\theta_{13} - \frac{\Delta m^2_{21}}{4E}\cos2\theta_{12}. \quad (10)$$

Straightforward calculations show that the derivative of $P_{3\times3}(\nu_e \to \nu_e)$ with respect to θ_{13} is negative for all solar neutrino energies if

$$P_{2\times2} - \frac{G_F N_e}{4\sqrt{2}}\cos2\theta_{12}\cos^2\theta_{13}\frac{(\frac{\Delta m^2_{21}}{4E}\sin2\theta_{12})^2}{[(\frac{\Delta m^2_{21}}{4E}\sin2\theta_{12})^2 + \phi^2]^{3/2}} - \tan^2\theta_{13} > 0. \quad (11)$$

In Fig. 1 we plot the quantity on the left-hand side of this inequality as a function of the neutrino production point denoted by its fractional radius x, for energies $E = 0.1$, 8, 18.8 MeV. N_e is evaluated from the data on ρ and X_H given in [22] with

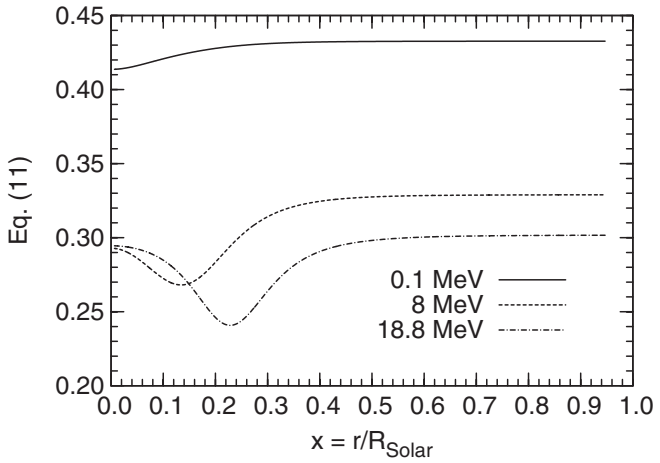

FIG. 1. The three lines represent expression (11) as a function of the neutrino production point for neutrino energies 0.1 MeV, 8 MeV, and 18.8 MeV with $\sin\theta_{13} = 0.13$. For all experimentally allowed values of θ_{13} the quantity plotted in this graph is positive implying that the survival probability is always a decreasing function of θ_{13}.

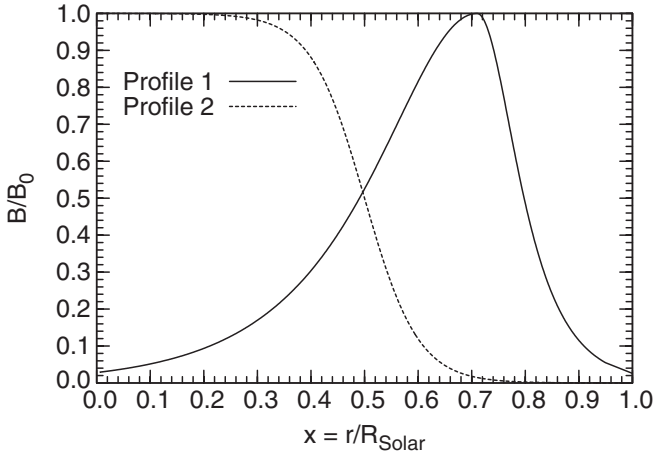

FIG. 2. The two solar field profiles given by Eqs. (13)–(15) normalized to their peak field values and expressed as a function of the fractional solar radius.

$$N_e = \frac{\rho}{m_p}\frac{1 + X_H}{2} \quad (12)$$

where ρ, m_p, and X_H are the density, the proton mass, and the hydrogen mass fraction. All neutrino parameters including θ_{13} were fixed at their best-fit central values [18]. The minimum of the quantity (11) is clearly seen in Fig. 1 for the three energy values considered and the central value $\theta_{13} = 0.13$ claimed in Ref. [18]. For $x = r/R_\odot$, this minimum reaches zero at $x \simeq 0.2$ as the energy is increased up to $E_{\max} = E_{\max}(\text{hep}) = 18.8\,\text{MeV}$ and θ_{13} up to 0.47 which is much above 3σ from its central value.[1] Thus we can conclude that for all experimentally allowed values of the physical quantities involved the condition (11) is satisfied and $P_{3\times3}(\nu_e \to \nu_e)$ is a decreasing function of θ_{13}.

B. Field profiles and rates

We base our numerical calculations for the rates on the standard solar model with high metalicity, BPS08(GS) [25]. As far as the solar field is concerned, solar physics provides very limited knowledge on its magnitude and shape. For instance in Ref. [26] upper bounds of 0.5–1.5 G and 30 G are quoted in the bottom of the convection zone and in the core, respectively, while in Ref. [27] an argument is presented favoring an upper bound of 600 G in the radiation zone. On the other hand, the authors of Ref. [28] estimate in the bottom of the convection zone an upper limit of 300 kG and in the midradiation zone and solar center a magnetic field strength of 0.7 MG and 7 MG, respectively [29].

Given the above-mentioned uncertainties we consider the two following plausible profiles which are approximately complementary to each other (see also Fig. 2)

[1]It has been recently pointed out [23,24] that the hint for a nonvanishing θ_{13} is at most a 1σ effect on the basis of present data.

Profile 1

$$B = \frac{B_0}{\cosh[6(x - 0.71)]} \quad 0 < x < 0.71 \tag{13}$$

$$B = \frac{B_0}{\cosh[15(x - 0.71)]} \quad 0.71 < x < 1 \tag{14}$$

Profile 2

$$B = \frac{B_0}{1 + \exp[10(2x - 1)]} \quad 0 < x < 1. \tag{15}$$

Profile 1 has a peak B_0 at the bottom of the convection zone, for fractional solar radius $x \simeq 0.71$, its physical motivation being the large gradient of angular velocity over this range [30]. It should not exceed 300 kG at this depth and 20 kG at 4–5% depth, hence its fast decrease along the convection zone [28]. Profile 2 is of the Wood-Saxon type, being maximal at the solar center. In this case the peak field B_0 could be as large as a few MG [31].

The survival probability was obtained from the numerical integration of the Schrödinger-like equation with Hamiltonian (7) using the Runge-Kutta method. All event rates (total and spectral) were evaluated as described in Refs. [32,33]. The expression for the ^{8}B spectral rate as applied to the Super-Kamiokande and Borexino experiments with three active neutrinos is now

$$R^{\rm th}_{\rm SK,Bor}(E_e) = \frac{\int_{m_e}^{E'_{emax}} dE'_e f_{\rm SK,Bor}(E'_e, E_e) \int_{E_m}^{E_M} dE \phi(E)[P_{ee}(E) \frac{d\sigma_e}{dT'} + (P_{e\mu}(E) + P_{e\tau}(E)) \frac{d\sigma_{\mu,\tau}}{dT'}]}{\int_{m_e}^{E'_{emax}} dE'_e f_{\rm SK,Bor}(E'_e, E_e) \int_{E_m}^{E_M} dE \phi(E) \frac{d\sigma_e}{dT'}} \tag{16}$$

where σ_e is the charged and neutral current cross section and $\sigma_{\mu,\tau}$ is the neutral current one. The energy resolution functions are given in [34,35] and the threshold energies $E_e = 5$ MeV, $E_e = 2.8$ MeV for Super-Kamiokande and Borexino, respectively. For the statistical analysis of all solar data (except Borexino) we used the standard χ^2 definition [32,33]

$$\chi^2 = \sum_{j_1, j_2} (R^{\rm th}_{j_1} - R_{j_1}{}^{\rm exp})[\sigma^2({\rm tot})]^{-1}_{j_1 j_2} (R^{\rm th}_{j_2} - R_{j_2}{}^{\rm exp}) \tag{17}$$

where indices j_1, j_2 run over solar neutrino experiments and the error matrix includes the cross section, the astrophysical, and the experimental uncertainties.

The rates we obtained were confronted with the data from the Cl experiment [8], the Ga ones [13], the Super-Kamiokande spectrum [6], the SNO rates and spectra [36], the Borexino spectra for ^{8}B neutrinos [17], and for the remaining fluxes [37].[2] Starting with profile 1 (Fig. 2) which peaks at the bottom of the convection zone, we considered the case of a relatively strong field and a vanishing one, and likewise for profile 2 (Fig. 2). Numerical results are insensitive to field values below 50 kG. In order to provide a feeling of the rates variation with θ_{13}, we also run this parameter from zero to 0.13. The values of the active sterile mass squared difference, which determines the location of the spin flavor resonance, were $\Delta m^2_{01} = m^2_0 - m^2_1 = 1.25 \times 10^{-7}$ eV^2 and $\Delta m^2_{01} = 2.7 \times 10^{-6}$ eV^2 obtained by fitting with profile 1 and profile 2, respectively, using the Landau-Zener approximation for the spin flavor precession resonance. For the ^{8}B flux normalization we used $f_B = 0.95$ [17] and the remaining neutrino parameters were [18]

$$\Delta m^2_{21} = 7.67 \times 10^{-5}\ {\rm eV}^2, \quad \Delta m^2_{23} = 2.39 \times 10^{-3}\ {\rm eV}^2, \quad \sin\theta_{12} = 0.559, \quad \sin\theta_{23} = 0.683. \tag{18}$$

Since, as explained below, our predictions refer to the average magnetic activity in the solar cycle, they should be evaluated for an intermediate field strength. Therefore we take $B_0 = 140$ kG for profile 1, while for profile 2 the peak value will be obtained from fitting. Regarding the mass basis magnetic moments $\tilde{\mu}_{1,2,3}$, we found that the numerical results are independent of which moment is chosen to be the largest. For the assumed peak field strength, the fits require this largest value to be $2 \times 10^{-12} \mu_B$. To this end the two-flavor (transition) moments $\mu_{(\mu,\tau)s}$ must be of order $1.4 \times 10^{-12} \mu_B$ with μ_{es} equal or arbitrarily smaller. A value $1.7 \times 10^{-12} \mu_B$ is also possible for the largest of the mass basis magnetic moments,[3] provided either $\mu_{\mu s}$ or $\mu_{\tau s}$ is as large as $1.4 \times 10^{-12} \mu_B$ with the other two no smaller than $1.0 \times 10^{-12} \mu_B$. In other words, $\mu_{(\mu,\tau)s}$ are the dominant moments that fix the amount of the active neutrino flavor suppression. In the following we will consider $\mu_{(\mu,\tau)s} \simeq 1.4 \times 10^{-12} \mu_B$ with μ_{es} arbitrarily equal or smaller, thus ensuring that the largest of the $\tilde{\mu}$'s is $\simeq 2 \times 10^{-12} \mu_B$.

C. Discussion

Starting with profile 1, the results for all solar neutrino experiments except Borexino, which is discussed below, are displayed in Table I (total rates and fluxes) and Fig. 3 (Super-Kamiokande spectral rate). They show a clear preference for a sizable magnetic field. We note that not only the flatness of the spectrum is enhanced thus providing a better fit to the data (see Fig. 3), but also the total rate predictions for the Cl, SK, and SNO experiments strongly

[2]We recall that, as mentioned in the Introduction, we neglect any possible time variation in the Ga rate and perform fits to its average value, see Ref. [13].

[3]This would however require $B_0 \simeq$ (160–170) kG.

TABLE I. Peak field values (profile 1), $\sin\theta_{13}$, total rates (in SNU for Ga and Cl experiments, in 106 $\mathrm{cm}^{-2}\,\mathrm{s}^{-1}$ for SK and SNO), and the corresponding χ^2's. The total number of degrees of freedom is 82 = 84 experiments (Ga + Cl + 44 SK + 38 SNO data points)—2 parameters, (see Ref. [15]). It is seen that for a sizable field (B_0 = 140 kG) all fits improve.

B_0 (kG)	$\sin\theta_{13}$	Ga	Cl	SK	$\mathrm{SNO_{NC}}$	$\mathrm{SNO_{CC}}$	$\mathrm{SNO_{ES}}$	χ^2_{rates}	$\chi^2_{\mathrm{SK_{sp}}}$	χ^2_{SNO}	χ^2_{gl}
0	0	67.2	2.99	2.51	5.62	1.90	2.49	0.07	42.7	57.2	99.9
	0.1	66.0	2.94	2.49	5.62	1.87	2.46	0.30	42.1	55.2	97.6
	0.13	65.0	2.90	2.46	5.62	1.84	2.44	0.62	41.7	53.7	96.0
140	0	66.4	2.82	2.32	5.37	1.76	2.31	0.20	37.6	46.0	83.8
	0.1	65.3	2.77	2.29	5.37	1.73	2.28	0.53	37.9	44.9	83.3
	0.13	64.3	2.72	2.27	5.37	1.70	2.25	0.95	38.4	44.1	83.4

improve (Table I). A strictly constant spectrum could on the other hand be obtained by varying the solar parameters Δm^2_{21} and $\sin\theta_{12}$ within a 2σ range. As for the Ga rate, vanishing and sizable fields are equivalent, as both classes of predictions lie within 1σ of the central value [13]. Moreover as to the magnitude of θ_{13}, the predictions do not show any clear preference. Altogether the results are more sensitive to changes in the solar parameters than in the atmospheric ones.

The Borexino spectral rate for ^{8}B is shown in Fig. 4. The top curve is the central value of the ratio between the best-fit recoil spectrum due to oscillated neutrinos and the spectrum due to nonoscillated ones evaluated from Fig. 3 of Ref. [17]. The next group of three curves represents the predicted spectra for vanishing field with $\theta_{13} = 0, 0.1, 0.13$ from top to bottom, respectively, and the bottom three curves represent the same but for a field (B_0 = 140 kG). The result of a χ^2 analysis with 4 degrees of freedom for vanishing field and profile 1 with B_0 = 140 kG is presented in the first three columns of Table II. Owing to the magnitude of the experimental errors, it is not possible to conclude whether the data shows any preference for a vanishing or a finite θ_{13}, although a sizable magnetic field appears to be disfavored. From Fig. 4 and Table II our predictions look more sensitive to the magnetic field variation than to the θ_{13} one within their respective allowed ranges. An improved significance can be obtained if Borexino are able to reduce their errors to 1/3 of the present ones (see the fourth column of Table II).

From the data and the model predictions presented, it is unclear whether Borexino can favor either a negligible or a sizable solar magnetic field. The available data from the remaining experiments appear to favor on the other hand a sizable field, possibly connected to a more intense solar activity in the convection zone. Hence it might be appropriate to examine the period in which the data were taken. In particular the Super-Kamiokande spectrum refers to the

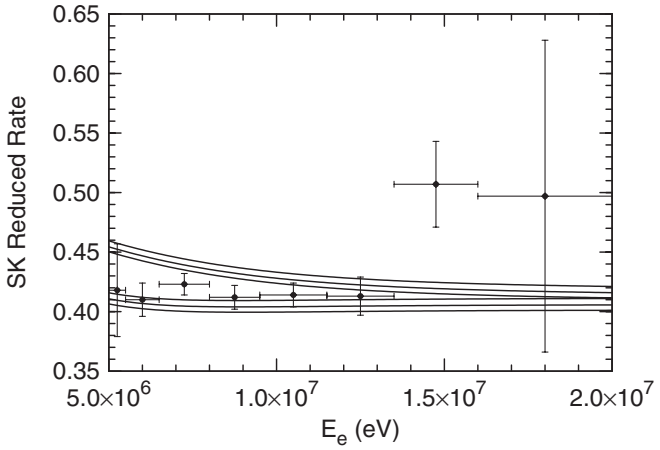

FIG. 3. The Super-Kamiokande spectrum: theoretical predictions and data points [6] normalized to BPS08(GS) [25]. The top three curves refer to $\sin\theta_{13} = 0, 0.1, 0.13$ from top to bottom in the case of zero magnetic field, and the lower three curves refer to the same values of $\sin\theta_{13}$ for a sizable field (profile 1), with B = 140 kG at the peak. There is a clear preference for a sizable field possibly related to solar activity, in comparison to a vanishing one. Units for the observed electron energy E_e are in eV.

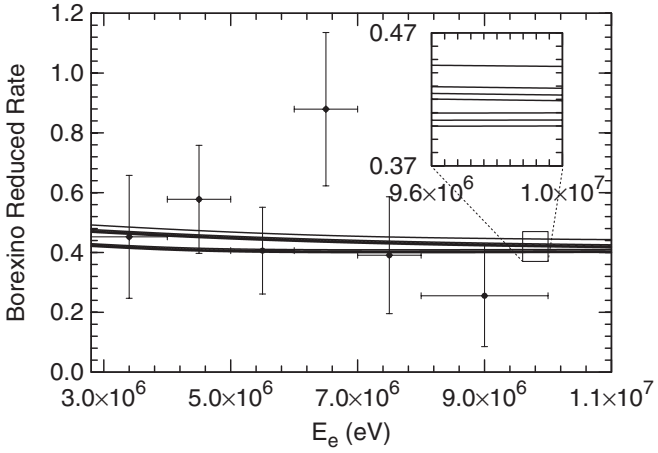

FIG. 4. The Borexino ^{8}B spectrum normalized to BPS08(GS) [25]. The top curve is extracted from Fig. 3 of Ref. [17] as explained in the main text. The lower two groups are from top to bottom the model predictions with $\sin\theta_{13} = 0, 0.1, 0.13$, $B = 0$ and $\sin\theta_{13} = 0, 0.1, 0.13$, B = 140 kG at the peak (profile 1). There is a preference in this case for a vanishing field possibly related to a quiet Sun. Notice that the theoretical curves coincide for $E_e > 5$ MeV with the corresponding ones in the previous figure apart from a minor difference due to the energy resolution functions.

TABLE II. The result of our χ^2 analysis for Borexino (profile 1): from the first three columns it is seen that no conclusion can be drawn as for the magnitude of $\sin\theta_{13}$ and that the significance is too low for the data to favor a vanishing field. The last column shows the χ^2 variation if the experimental error were reduced to 1/3, so a vanishing field would clearly be favored. The result would still in this case be inconclusive regarding the size of $\sin\theta_{13}$.

B_0 (kG)	$\sin\theta_{13}$	χ^2	$\Delta\chi^2$
0	0	4.55	0
0	0.095	4.55	0
0	0.13	4.56	0
140	0	4.93	2.4
140	0.095	4.98	2.5
140	0.13	5.03	2.6

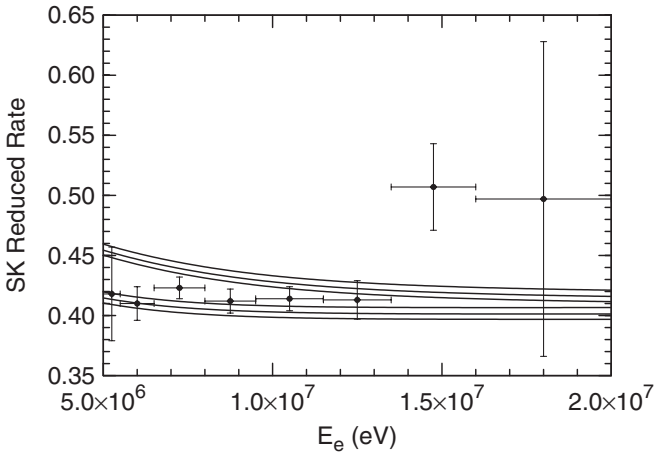

FIG. 5. Same as Fig. 3 with the three bottom curves referring to profile 2 with $B = 0.75$ MG at the peak.

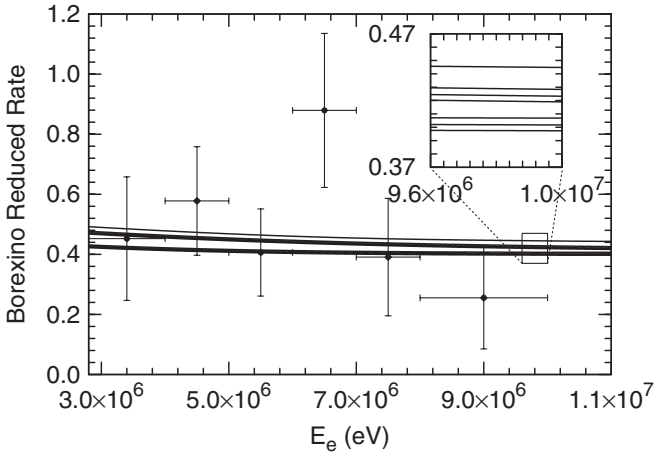

FIG. 6. Same as Fig. 4 (^{8}B Borexino spectra) for profile 2.

period from May 31, 1996 to July 15, 2001 during which the average sunspot number was 65. On the other hand the Borexino ^{8}B spectrum refers to a data-taking period from July 15, 2007 to June 21, 2008 with average sunspot number 4 [38]. In most of the former period the solar magnetic activity increased and reached an 11-year peak in the summer of 2000, whereas in the latter the activity was continuously at its minimum. Therefore in light of the present model, one expects the present Borexino spectrum for ^{8}B to coincide with the LMA prediction and the Super-Kamiokande one to reflect an active Sun.

We have also tested the model for the remaining fluxes observed in the first Borexino phase [37], including in addition the pp and pep neutrinos. In this case $E \leq 1.7$ MeV for all fluxes, so that with $\Delta m^2_{01} = 1.25 \times 10^{-7}$ eV^2 all neutrino resonances lie below $x = 0.5$ where the magnetic field strength is $B < \frac{1}{2}B_0$ (see Fig. 2). Furthermore since the matter density is larger in this range, the variation of the field besides being smaller, becomes much less important. The maximum variation that is reflected in the event rates is no greater than 1%, hence, given the order of magnitude of the experimental errors which is about 25% [37], it cannot be expected to be seen in this case for any flux. We may therefore conclude that it is of prime importance that Borexino will continue monitoring both the low-energy and the ^{8}B flux during the present increasing solar activity period.

While it is generally accepted that the sunspot activity is interrelated with the possible modulation of the convection zone magnetic field, no connection appears to exist between such varying activity and the radiation and core magnetic field. There is, however, a recent claim in the literature [2] suggesting the existence of an inner tachocline separating the core from the radiation zone and an inner dynamo producing a strong magnetic field and a second solar cycle. Independently of the fact that our knowledge on this matter that can be obtained from solar physics is very limited at present, it will be shown in the following that the solar neutrino data are consistent with a varying field in these inner regions.

TABLE III. Same as Table I for profile 2 where the vanishing field case is omitted. As for profile 1, with a sizable field ($B_0 = 0.75$ MG), all fits improve with relation to the vanishing field (compare with Table I).

B_0 (MG)	$\sin\theta_{13}$	Ga	Cl	SK	$\mathrm{SNO_{NC}}$	$\mathrm{SNO_{CC}}$	$\mathrm{SNO_{ES}}$	χ^2_{rates}	$\chi^2_{\mathrm{SK_{sp}}}$	χ^2_{SNO}	χ^2_{gl}
0.75	0	64.7	2.75	2.32	5.38	1.76	2.32	0.76	38.0	46.1	84.8
	0.1	63.6	2.70	2.30	5.38	1.73	2.29	1.32	38.4	45.0	84.7
	0.13	62.6	2.66	2.28	5.38	1.70	2.26	1.92	38.8	44.2	84.9

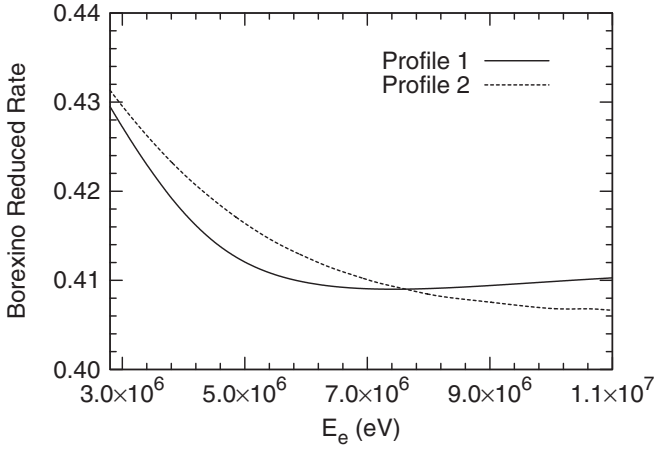

FIG. 7. Borexino spectra for ^{8}B neutrinos evaluated for profiles 1 and 2 at the best fit with $\theta_{13} = 0$ (parameter values as in the main text). The spectrum for profile 1 exhibits a shallow minimum while for profile 2 it is monotonically and smoothly decreasing with the energy.

Referring to profile 2 [Eq. (15) and Fig. 2] and in order that a possible time modulation may be detected, all resonances from active to sterile must be located deeper inside the Sun with relation to profile 1, so that the shift from a weak to a strong field or vice versa is reflected in the intensity of the neutrino flux. In this way the best fit to the data was obtained for $\Delta m^2_{10} = 2.7 \times 10^{-6}$ eV^2 and $B_0 = 0.75$ MG[4] with the remaining neutrino parameters as in Eq. (18). The results for the total rates and fluxes are now shown in Table III and those for the Super-Kamiokande and ^{8}B Borexino spectra in Figs. 5 and 6.

Again, as for profile 1, the Super-Kamiokande data show a clear preference for a large field (Fig. 5), and the quality of the fits is the same for both profiles. As can be seen from a comparison between Figs. 3 and 5 or Figs. 4 and 6, the spectra for a sizable peak field are much alike, and it will be very hard to experimentally distinguish between them in this way. The actual difference can be explicitly seen in Fig. 7 where the Borexino spectrum for both profiles is shown for $\theta_{13} = 0$ with the remaining parameters as in Tables I and III. Whereas for profile 1 the spectrum presents a shallow minimum around $E = 8$ MeV, it decreases monotonically in the case of profile 2. We have also seen that in the case of profile 2 the results are less stable, in the sense that small variations either in the neutrino parameters Δm^2_{21} and θ_{12} or B_0 lead to larger variations in the rates and fits. Similarly to profile 1, the results for a χ^2 analysis for profile 2 are shown in Table IV and the case for a vanishing or a sizable field is again inconclusive.

[4]For instance with $\Delta m^2_{10} = 1.25 \times 10^{-7}$ eV^2, the neutrinos with energy $E = 5$ MeV have their resonance at $x = 0.64$ whereas for $\Delta m^2_{10} = 2.7 \times 10^{-6}$ eV^2 this resonance moves to $x = 0.34$.

TABLE IV. The same as Table II for profile 2. The fourth column indicates the χ^2 variations relative to its values for the vanishing field given in the first three rows of Table II.

B_0 (MG)	$\sin\theta_{13}$	χ^2	$\Delta\chi^2$
0.75	0	4.93	1.9
0.75	0.095	4.89	1.8
0.75	0.13	4.84	1.7

Finally for profile 2 we have calculated the rates corresponding to the remaining fluxes which were observed in the first Borexino phase [37]. For all these neutrinos, with $E \leq 1.7$ MeV, the corresponding resonances lie in the range $x < 0.23$ where the field is close to maximal. Thus the event rate modulation is expected to be much stronger than with profile 1. It is now approximately 9% which we believe to be within reach of the Borexino experiment in the future. The results are shown in Fig. 8 where we chose to represent the modulation of the ^{7}Be, ^{15}O, and ^{13}N fluxes. Owing to the magnitude of the errors involved ($\simeq 25\%$), the χ^2, of order 38 (51 d.o.f.), is extremely flat for both profiles and it is hard to distinguish any preference of the data at all either for profile 1 or 2. So it is also of prime importance to keep Borexino monitoring the low-energy neutrino fluxes too, namely ^{7}Be and CNO as in the first phase. Therefore solar neutrino experiments hold the potential to clearly trace a field modulation inside the Sun and moreover possibly to distinguish whether this modulation occurs in the convection zone or deeper in the radiation zone and core.

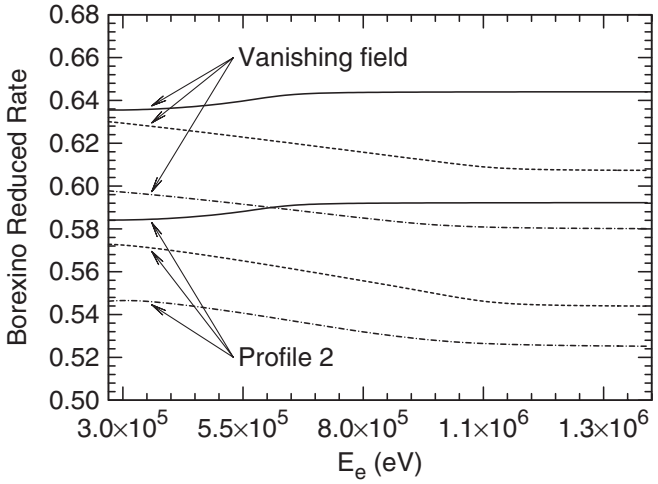

FIG. 8. Borexino spectra for ^{7}Be neutrinos (full lines), ^{15}O (dashed), and ^{13}N (dot-dashed) evaluated for vanishing field and profile 2 at the best fit with $\theta_{13} = 0$ (parameter values as in the main text).

IV. SUMMARY AND CONCLUSIONS

We have developed a model with three active neutrino flavors communicating to a sterile one in matter with magnetic field through transition magnetic moments. Its motivation is to provide better fits to the solar neutrino data than the LMA ones, in particular, a flat Super-Kamiokande spectrum and a better prediction for the Chlorine rate, while keeping accurate predictions for all other rates including the recent ^{8}B Borexino spectrum. We investigated two magnetic solar field profiles, one which peaks at the bottom of the convection zone and another at the solar center. These represent two classes of plausible possibilities which somehow complement each other.

The starting point was the derivation of the (4×4) Hamiltonian followed by a simple and general argument showing that the survival probability is a decreasing function of the still unknown mixing angle θ_{13}. This fact, which is reflected more strongly in the charged current data, leads to a parallel shift of the spectral event rates. This shift is however not enough to distinguish a clear preference of the data between a vanishing or a sizable θ_{13}.

We found that among the three transition moments, the ones connecting ν_μ and ν_τ to the sterile are the dominant ones that fix the amount of active flavor suppression. They are both required to be of order $1.4 \times 10^{-12}\mu_B$, while ν_{es} may be equal or arbitrarily smaller. Alternatively either ν_μ or μ_τ separately may be of order $1.4 \times 10^{-12}\mu_B$ with the remaining two of order $1.0 \times 10^{-12}\mu_B$ in which case a slightly stronger field is required.

On the other hand it was found that all experimental data, with the exclusion of the Borexino ones, favor a relatively large magnetic field of either class. To this end it is important to realize that the former data are average ones and refer to extended periods. In particular the Super-Kamiokande spectrum refers to a period when the average solar magnetic activity was relatively intense, and hence it is sensible to expect it to be flat in a way that it reflects a large field in accordance with the model predictions. As regards the Borexino spectrum in a similar energy range, it is not possible at present to conclude whether it favors the LMA spectrum or the LMA one with spin flavor precession, as the data errors are too large.

Whereas the neutrino fluxes observed in the first Borexino phase were found to be insensitive to field modulations in the convection zone (profile 1), this is not so if the field is concentrated in the core and radiation zone (profile 2). The event rate modulation expected in this case is of the same magnitude as the one expected for the ^{8}B flux with any of the profiles. Hence we believe it extremely important to keep Borexino taking data for all neutrino fluxes during at least the first half of the present solar cycle expected to peak in 2011 or 2012.

TABLE V. The possibility for detecting through solar neutrino experiments the magnetic fields concentrated either in the convection zone (profile 1) or in the core and radiation zone (profile 2).

Varying field	^{8}B flux	Others
Profile 1 (CZ)	Yes	No
Profile 2 (WS)	Yes	Yes

Our claim is not that there is evidence of variability of the solar field profile in the convection zone or equivalently in the core and radiative zone, but rather that the neutrino data are consistent with the possibility of either phenomenon.

Our results concerning field profiles and data variability are qualitatively summarized in Table V: a magnetic field concentrated around the bottom of the convection zone like profile 1 can only show its modulation through an experiment monitoring the high-energy ^{8}B flux, whereas a field concentrated in the core and radiation zone like profile 2 can be detected by experiments monitoring either the high-energy ^{8}B or the low-energy fluxes.

To conclude, solar neutrino experiments may hold a non-negligible potential to ascertain whether there is a varying magnetic field inside the Sun possibly connected to solar activity, a fact which otherwise may be very difficult to establish on the basis of solar physics alone. Moreover, we have shown that it is also possible to trace whether this varying field is lying mostly at the bottom of the convection zone or deeper in the core and radiation zone.

ACKNOWLEDGMENTS

C. R. Das gratefully acknowledges support from Fundação para a Ciência e Tecnologia ref. SFRH/BPD/41091/2007. One of us (M. P.) is grateful to D. Montanino for useful discussions.

[1] P. A. Sturrock, arXiv:0810.2755.
[2] P. A. Sturrock, arXiv:0805.3686.
[3] L. Pandola, Astropart. Phys. **22**, 219 (2004).
[4] P. A. Sturrock and D. O. Caldwell, Astropart. Phys. **26**, 174 (2006).
[5] S. Fukuda *et al.* (Super-Kamiokande Collaboration), Phys. Rev. Lett. **86**, 5651 (2001).
[6] S. Fukuda *et al.* (Super-Kamiokande Collaboration), Phys. Lett. B **539**, 179 (2002).
[7] P. Anselmann *et al.* (GALLEX Collaboration), Phys. Lett.

B **285**, 390 (1992).
[8] B. T. Cleveland *et al.*, Astrophys. J. **496**, 505 (1998).
[9] P. C. de Holanda and A. Y. Smirnov, Phys. Rev. D **69**, 113002 (2004).
[10] C. S. Lim and W. J. Marciano, Phys. Rev. D **37**, 1368 (1988).
[11] E. K. Akhmedov, Phys. Lett. B **213**, 64 (1988).
[12] B. C. Chauhan and J. Pulido, J. High Energy Phys. 06 (2004) 008.
[13] C. Cattadori, N. Ferrari, and L. Pandola, Nucl. Phys. B, Proc. Suppl. **143**, 3 (2005).
[14] V. N. Gavrin and B. T. Cleveland, arXiv:nucl-ex/0703012.
[15] B. C. Chauhan, J. Pulido, and M. Picariello, J. Phys. G **34**, 1803 (2007).
[16] V. A. Koutvitsky, V. B. Semikoz, and D. D. Sokoloff, Astron. Zh. **86**, 1 (2009).
[17] G. Bellini *et al.* (Borexino Collaboration), arXiv:0808.2868.
[18] G. L. Fogli *et al.*, Phys. Rev. D **78**, 033010 (2008).
[19] C. Amsler *et al.* (Particle Data Group), Phys. Lett. B **667**, 1 (2008).
[20] G. L. Fogli, E. Lisi, D. Montanino, and A. Palazzo, Phys. Rev. D **62**, 013002 (2000).
[21] A. B. Balantekin and H. Yuksel, J. Phys. G **29**, 665 (2003).
[22] http://www.sns.ias.edu/jnb/.
[23] T. Schwetz, M. Tortola, and J. W. F. Valle, New J. Phys. **10**, 113011 (2008).
[24] M. Maltoni and T. Schwetz, arXiv:0812.3161.
[25] C. Pena-Garay and A. Serenelli, arXiv:0811.2424.
[26] Nicholas Boruta, Astrophys. J. **458**, 832 (1996).
[27] L. L. Kitchatinov, Astro. Rep. **52**, 247 (2008).
[28] H. M. Antia, S. M. Chitre, and M. J. Thompson, Astron. Astrophys. **360**, 335 (2000).
[29] H. M. Antia, J. Astrophys. Astron. **29**, 85 (2008).
[30] H. M. Antia, S. Basu, and S. M. Chitre, arXiv:0803.3619.
[31] T. I. Rashba, V. B. Semikoz, S. Turck-Chieze, and J. W. F. Valle, Mon. Not. R. Astron. Soc. **377**, 453 (2007).
[32] J. Pulido and E. K. Akhmedov, Astropart. Phys. **13**, 227 (2000).
[33] J. Pulido, Astropart. Phys. **18**, 173 (2002).
[34] Y. Fukuda *et al.* (Super-Kamiokande Collaboration), Phys. Rev. Lett. **81**, 1158 (1998); **81**, 4279(E) (1998).
[35] D. Montanino, M. Picariello, and J. Pulido, Phys. Rev. D **77**, 093011 (2008).
[36] B. Aharmim *et al.* (SNO Collaboration), Phys. Rev. C **72**, 055502 (2005).
[37] C. Arpesella *et al.* (Borexino Collaboration), Phys. Lett. B **658**, 101 (2008).
[38] http://www.solen.info/solar/solcycle.html.